Citation: Li, Y., Wang, H., Zhu, J.Q., Zhang, G.T., Guo, H., Li, X.H., Lin, S., Min, J., 2022. Depositional evolution and models for a deep-lacustrine gravity flow system in a half-graben rifted sag, Beibuwan Basin, South China Sea. Geologica Acta, 20.3, 1-18. DOI: 10.1344/GeologicaActa2022.20.3

geologica acta

Depositional evolution and models for a deep-lacustrine gravity flow system in a half-graben rifted sag, Beibuwan Basin, South China Sea

Yuan Li[1, 2] Hua Wang[3] Jie Qiong Zhu[4] Guo Tao Zhang[5*] Hao Guo[4] Xiao Han Li[4] Song Lin[1, 2, 6] Jin Min[1, 2]

[1]Institute of Seismology, CEA
Wuhan, 430071, China

[2]Key Laboratory of Earthquake Geodesy, CEA
Wuhan, 430071, China

[3]Faculty of Earth Resources, China University of Geosciences
Wuhan, 430071, China

[4]China Southern Petroleum Exploration & Development Corporation
Haikou, 570216, China

[5]Wuhan Institute of Geology and Mineral Resources, Chinese Academy of Geological Sciences
Wuhan, 430205, China

[6]Wuhan Institute of Earthquake Engineering Co., Ltd
Wuhan, 430071, China

*Corresponding author

ABSTRACT

The Paleogene Liushagang Formation is part of the Fushan Sag, a continental lacustrine basin located at the Southeastern margin of the Beibuwan Basin, South China Sea. Further understanding of the deep-water gravity flow deposits in this formation will be conducive to lithologic reservoir exploration in the sag. In this study, three members of the Liushagang Formation, SQEls3, SQEls2 and SQEls1, from old to young, are used with core observation, well log data, and three-dimensional seismic data to identify four deep-lacustrine gravity flow lithofacies including their vertical and lateral relationships within the depositional system. The results are then used to establish a deep-water gravity flow depositional model. Four types of gravity flow lithofacies developed in the sag: sandy debrite, turbidite, sandy slump, and bottom-current deposits. Sand-rich sub-lacustrine fan deposits with typical turbidite channels developed mainly in the western depression, whereas distal isolated lobes formed by sandy debrite flow deposits occurred mainly in the eastern depression. The results obtained in this study will be helpful in the research of gravity flows in similar continental lacustrine environments.

KEYWORDS **Deep-lacustrine gravity flow. Turbidity current. Sandy debrite. Fushan Sag. Beibuwan Basin.**

INTRODUCTION

Gravity flow deposits characterized by coarse-grained sandy material, are widely developed in semi-deep–deep lacustrine (sea) environments (Li *et al.*, 2019). Many researchers have reported gravity flow reservoirs in deep-lacustrine basins such as the Songliao (Pan *et al.*, 2017) and southern Ordos basins (Yang *et al.*, 2014) as well as in the Jiyang depression of the Bohai Bay Basin (Liu *et al.*, 2017; Xian *et al.*, 2016; Yang *et al.*, 2015). Forel (1887) proposed high density flow for the bottom currents of the Rhône River to Lake Geneva. The structural sequence of this density flow was further detailed by Sheldon (1928), and the concept of turbidity current was proposed by Johnson (1938). Bouma (1962) and Walker (1978) established the classical Bouma sequence and sub-marine fan model according to the vertical sedimentary sequence and spatial distribution characteristics of gravity flows. While questioning the traditional turbidity current theory, Shanmugam (1996, 1997) reviewed developments in gravity flow research of the previous 50 years and put forward the concept of sandy debris flow. He established two types of deep-water slope models, non-channel and channel systems, corresponding to mud-rich and sand-rich continental shelves, respectively (Shanmugam, 2000, 2013). However, sedimentary patterns differ among regions owing to the sedimentary structure background, gravity flow formation, and triggering mechanism. Therefore, to establish a suitable depositional model for deep-lacustrine gravity flow reservoirs, attention should be given to the sedimentary characteristics of the study area.

The Fushan Sag, a Cenozoic sedimentary sag filled with continental and marine deposits, includes the lacustrine facies-dominated Paleogene Liushagang Formation, which accumulated a thickness of 117-2452m during the rifting period (He *et al.*, 2006; Shi *et al.*, 2007) (Fig. 1A). In a previous study, we applied the sequence stratigraphy of Vail (1987) to identify the Liushagang Formation Sequence as a complete second-order sequence unit (Li *et al.*, 2014; Ma *et al.*, 2012) including T_7 and T_4 as the bottom and top boundaries of the sequence, respectively. In addition, three third-order sequence units were identified in decreasing age as the third, second, and first members of the Liushagang Formation, represented by SQEls3, SQEls2, and SQEls1, respectively. The bottom and top boundaries of SQEls2 were identified as T_6 and T_5, respectively (Figs. 1A; 2D). During the SQEls2 period, the deep-lacustrine area expanded rapidly and created conditions enabling gravity flow deposition, which offers strong exploration potential (Li *et al.*, 2010; Wang *et al.*, 2014). Liu *et al.* (2000, 2003) proposed that the gravity flow deposits of SQEls2 formed a sub-lacustrine fan, which they divided into three units of gravity flow depositional facies: turbidite sedimentation, underwater debris flow deposition, and slump accumulation. However, our understanding of the deep-lacustrine gravity flow system of SQEls2 remains unclear owing to variations in seismic data acquisition and resolution.

The present study is based on information including drill core, drilling logging, and three-dimensional seismic data relevant to the main research area. It should be noted that the largest scale transgression of the Paleogene occurred during the SQEls2 period and formed deep-lacustrine mudstone throughout the sag, which made it difficult to identify the transgressive surface (ts) of this period (Fig. 1B). Accordingly, we traced the maximum flooding surface (mfs) through the entire sag and studied the lowstand and extension system tracts (SQEls2EST + LST) as the combined target layer. Therefore, the present study aims to i) characterize the deep-lacustrine gravity flow lithofacies of the SQEls2EST + LST period, ii) combine vertical and horizontal lithofacies analysis with that of the depositional system distribution and iii) establish deep-water gravity flow depositional models for the Fushan Sag. Our research is expected to promote petroleum exploration of the Paleogene Liushagang Formation in the Fushan Sag and to provide geological support for improving the success rate in the area's oilfields.

GEOLOGICAL SETTING

The Fushan Sag is located at the southern margin of the Beibuwan Basin, which is adjacent to the Hainan uplift and the Qiongzhou Strait to the South and North, respectively (Fig. 2A, B). The sag is a NE-E-trending half-graben sag filled with more than 9,000m of Cenozoic strata in an area of approximately 3,000km^2 (Kang *et al.*, 1994; Shi *et al.*, 2007). Owing to the influence of Yanshanian tectonics, numerous complex structures characterized by extensional, rotational, and strike–slip faults are developed in the sag. The Central Transition Zone, a low uplifted region located in the middle of the Fushan Sag, divides the sag into two independent sub-sags known as the eastern depression and the western depression, respectively (Fig. 2C). Our study area covers four sub structural units in the sag: the southern slope zone, the western depression, the Central Transition Zone and the eastern depression (Fig. 2C; D). During the development of the Liushagang Formation, the main source of the sediment was the southern Hainan uplift. The entire study area forms a wide domain gently tilted to the South and steep terrain in places (Ma *et al.*, 2012) (Figs. 2C; D). The extensional fracturing of the sag has been enhanced since the Paleogene under the influence of the South China Sea movement, volcanism and earthquakes. The volcanic activity is interpreted to include multiple eruptions of high intensity and long duration that occurred in a wide distribution range (Lin *et al.*, 2015). Volcanic rock units reached a maximum thickness of 220m in a single well

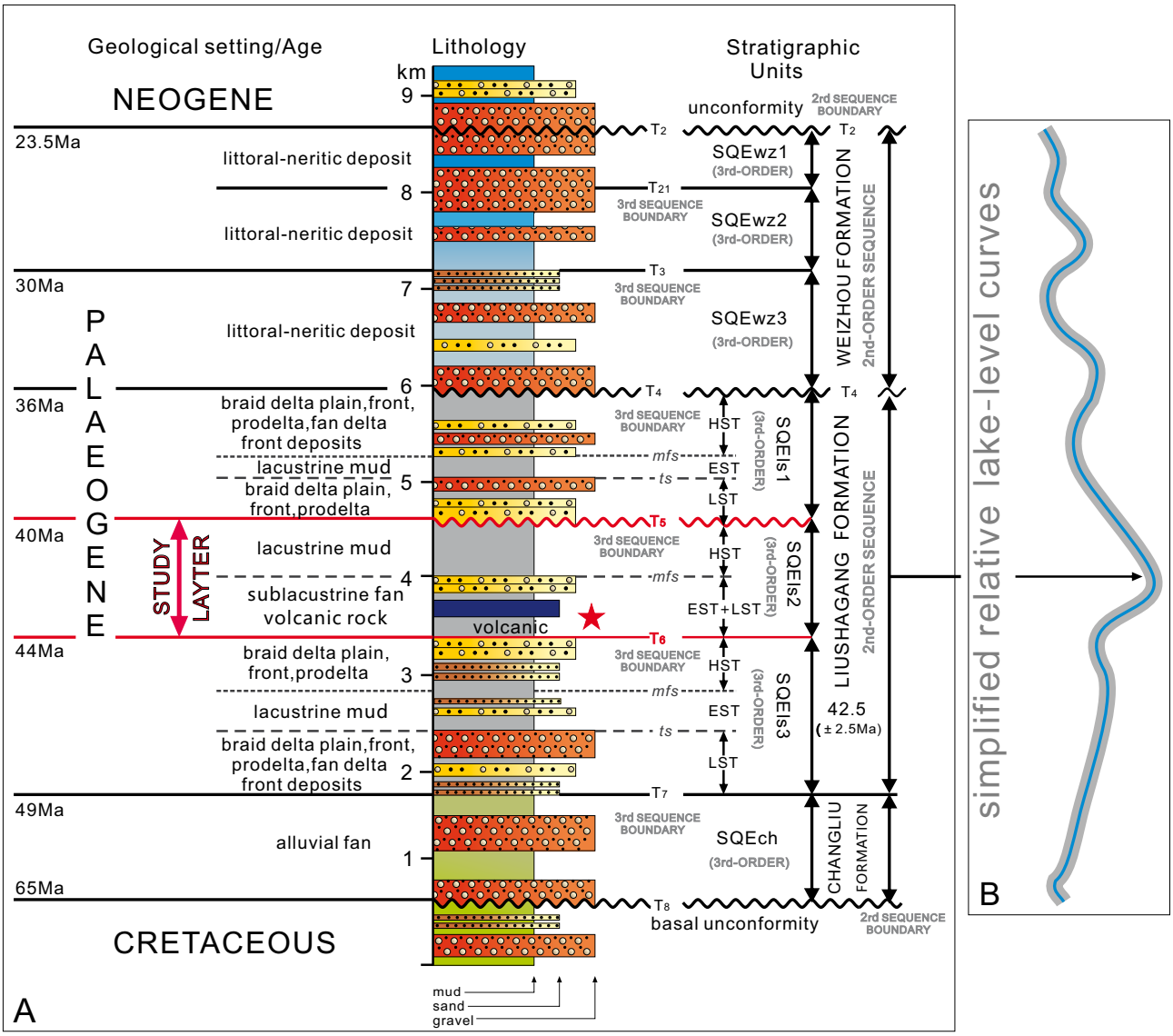

FIGURE 1. A) General stratigraphy of the Palaeogene infill of the Fushan Sag (Li *et al.*, 2014; Ma *et al.*, 2012 modified). Abbreviations include ts: transgressive surface; mfs: maximum flooding surface; LST: lowstand systems tract; EST: extension systems tract; HST: highstand systems tract. B) Simplified relative sea-level curve representing the three extension second-order cycles of the early, middle and late Palaeogene, respectively.

developed during the SQEls2 period. Overall, the abundant source system, slope structure, and frequent volcanic and seismic activities provided the necessary conditions for the development of deep-lacustrine gravity flow deposits in the Fushan Sag.

DESCRIPTION OF LITHOFACIES

The data used for this analysis were provided by the China Southern Petroleum Exploration & Development Corporation. The data of 16 cores obtained in the deep-lacustrine area of the Fushan Sag (Fig. 2C), each 218m in length, were used to identify four lithofacies of deep-lacustrine gravity flows that occurred during the SQEls2EST + LST period: sandy debrite, turbidite, sandy slump and bottom-current deposits (Fig. 3). These four types are defined according to their fabric, genetic mechanism, and rheological characteristics of sediments (Table 1).

Lithofacies 1 (*Lf*1): sandy debrite

According to its rheology, the sandy debris flow of *Lf*1 behaves as a Bingham plastic fluid, characterised by the continuous interaction between viscous and non-viscous debris flows (Xian *et al.*, 2012) (Fig. 3; Table 1). Elverhoi (2015) used flume experiments to demonstrate that gravity flows deposited during the same period contain turbidity

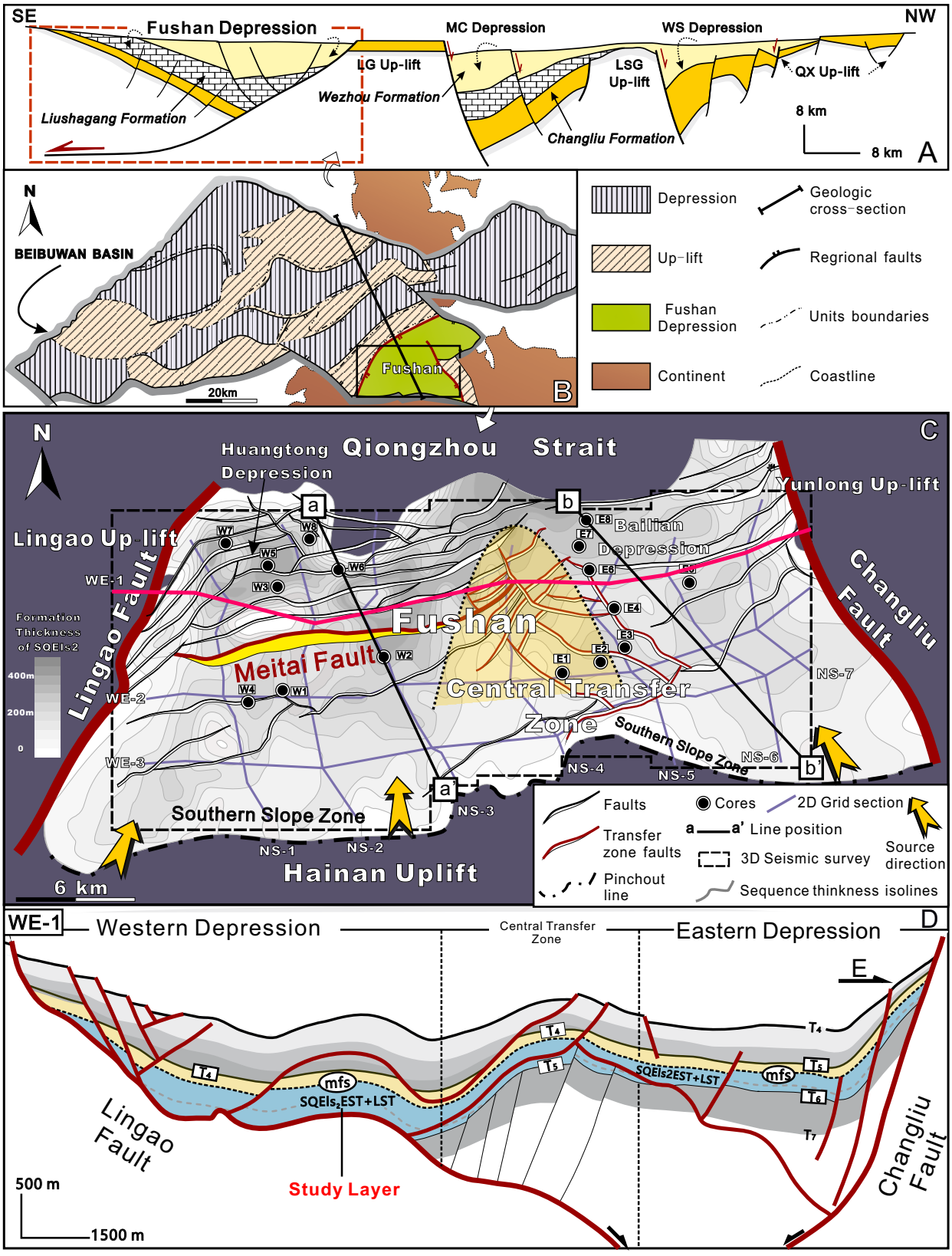

FIGURE 2. A) Geological profile across the Beibuwan Basin showing the major stratigraphy and the location of the Fushan Sag. B) Simplified map showing the tectonic framework of the Beibuwan Basin and the location of the Fushan Sag. C) Geological map of the Fushan Sag, showing the thickness of SQEIs2 and the distribution of major faults, secondary structures, and wells. D) Stratigraphic cross-section (along line WE-1) showing the stratigraphy of SQEIs2.

TABLE 1. Four deep-lacustrine gravity flow lithofacies of SQEls2ESL + LST

Facies	Lithology	Grain size	Grading	Bed thickness	Sedimentary structures	Secondary features	Sedimentary processes	Depositional environment
*Lf*1	Medium- to thick-bedded massive sandstone	Generally fine- to medium-grained sandstone, low mud matrix	No grading or inverse grading	0.2 to about 2.5 m	Basal shear zone, generally clean structureless sandstone, planar lamination rare, random floating mudstone clasts	Inverse grading commonly appear with sharp upper contact, planar clast fabric distribut in the upper sandstone, tongue-like planform geometry	Sandy debris flow	High energy setting; slope to base of slope
*Lf*2	Thin- to medium-bedded sandstone and siltstone	Fine- to very fine- grained sandstone, siltstone and mudstone;high mud matrix	Normal grading	0.02 to 0.25 m	Planar and parallel lamination,ripple cross-lamination	Sharp or erosional basal contact, gradational upper contact, lenticular geometry	Turbidity current	Moderate energy setting; found within channels and at base of basin
*Lf*3	Medium- to thick-bedded mixed sandstone	Generally medium-grained sandstone, high mud matrix	No grading	0.25 to 1.5 m	Scour bases rare, erosive bases, high degree of contortion and soft deformation, amalgamation	Irregular upper contact, tensional faults, compressional folding and associated sand injections	Sandy slump	High energy setting; slope with necessary gradient
*Lf*4	Thin- to very thin-bedded sandstone, siltstone and mudstone	Very fine-grained sandstone, siltstone and mudstone; high mud matrix	Inverse grading	<0.18 m	Parallel lamination, ripple cross-lamination, starved ripple lamination; double mud layers	Variable to complete bioturbation	Bottom current reworking	Low energy setting; found at base of basin and at top of sandy debrites

flows, with lower density distributed mainly at the top and front of the fluid and sandy debris flow with higher density occurring at bottom. This explains why the thick sandy debrite in *Lf1* was deposited in the slope area of the basin.

As shown in Figure 4, several main identification marks of *Lf*1 in the Fushan Sag were noted. In particular, floating mud gravel is present at the top of the core, which forms an irregular contact surface, and clean, massive sandstone with a shear zone occurs at the bottom. In addition, lath debris is present locally. The most typical characteristics of the sandy debris flow deposited during the SQEls2 period are gray and white fine to medium massive, clean sandstone, local mud gravel, lack of bedding structure and shear zone at the bottom, and low mud content. The mud gravel has a maximum particle size of 10cm and is arranged disorderly at the top of the sandstones. This lithofacies is distributed mainly in the eastern depression and is rarely developed in the western deep-lacustrine area.

Lithofacies 2 (*Lf*2): turbidite

The turbidity current forming *Lf*2 turbidites corresponds to a Newtonian fluid, with sediment suspended and transported by turbulence; the main deposition type is hindered sedimentation (Johnson, 1938). The massive sandstone in the core in segment A of the Bouma sequence, particularly the massive sandstone with floating mud gravel, should be interpreted as sandy clastic flow rather than high-density turbiditic current according to their formation characteristics and rheology (Fig. 3; Table 1). According to Shanmugam (1997), only the C–D–E–F segments of Bouma sequence can be interpreted as turbidite deposits.

In the study area, *Lf*2 (Fig. 5) is composed of a thin middle layer of fine sand to siltstone with a positive grain order. Sand-mud inter-bedding and horizontal bedding are well developed. Occasional climbing ripples were observed in segment C of the Bouma sequence, which shows that the water flow rate was lower than the sedimentation rate. The lower part of a complete positive grain order shows an obvious distinct interface. The lithofacies is distributed mainly in the western depression and occurs less often in the eastern sag. This is contrary to previous research by Liu *et al.* (2000, 2003), who proposed that a turbidite fan developed over the entire sag. It is worth noting that *Lf*1 in association with *Lf*2 was also observed in cores obtained near the slope in the western region.

Lithofacies 3 (*Lf*3): sandy slump

The sandy slump representing *Lf*3 is described as a light-gray, medium sandstone with with twisted laminations and mudstone intercalations that exhibit high angular and twisted deformation structures that occur (Fig. 3; Table 1). Shear zones, irregular top contact, tensile faults, compressional folds, and related intrusive sandstone veins occur commonly at the bottom of the unit (Fig. 6). Slumped sandstones associated with deformational structures were previously described in Lake Baikal, which is the deepest lake basin in the world, and was designated by Shanmugam *et al.* (2009) as an independent sedimentary facies type. Steep strata represent synsedimentary collapse and sandstone dykes formed from fracturing and liquefaction of sediments under the action of earthquakes. The shear zone and microfolding at the bottom of some massive sandstone might be secondary structures caused by shear stress and sliding of the massive sandstone on its basal contact. Because these sandy slump rocks deposited during the SQEls2EST + LST period are often associated with the sandy debrite of *Lf*1, it is difficult to distinguish them in some cores. *Lf*3 developed mainly in the deep-lacustrine area of the eastern depression.

Lithofacies 4 (*Lf*4): bottom-current deposits

The tractive sedimentary structure is a developmental feature of lithofacies *Lf*4 (Shanmugam *et al.*, 1993) (Fig. 3; Table 1), which forms from bottom-current flow. The rock of this lithofacies is composed of medium-gray, unconsolidated, very fine-grained sandstone with double mud layers (Fig. 7) occurring regularly in the eastern basin-floor area as inter-bedded fine sandstones and mudstones. The thickness of each unit changes from a few centimeters to nearly 1m in this lithofacies, which appears in vertical association with *Lf*2.

Rhythmic bedding and double-layered mudstone are diagnostic signatures of bottom-current processes

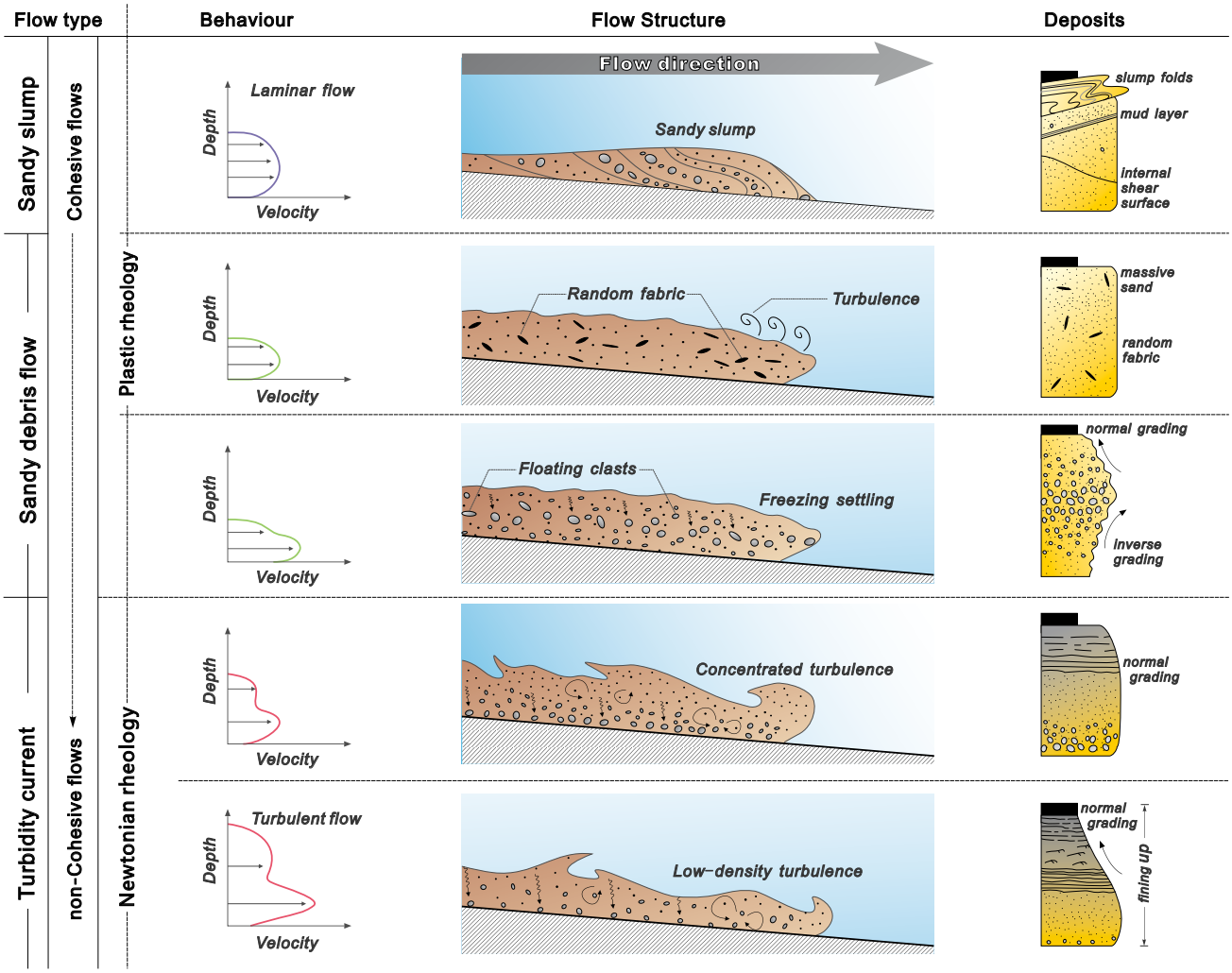

FIGURE 3. Classification scheme for deep-lacustrine gravity flow of SQEls2ESL + LST (the lowstand and extension system tracts of SQEls2), after Elverhol (2015), Johnson (1938), Shanmugam *et al.* (1993, 1997, 2009) and Xian *et al.* (2012).

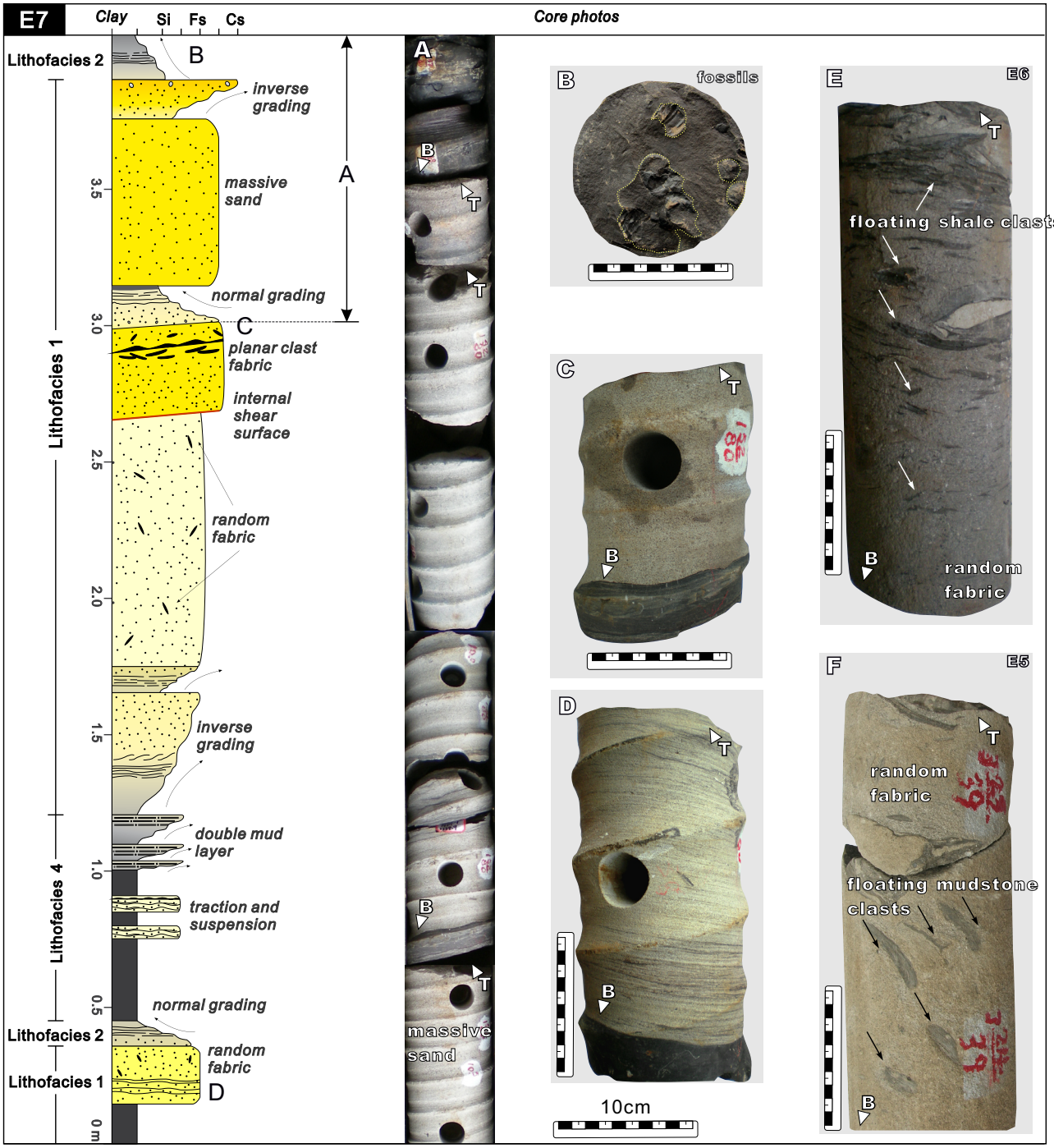

FIGURE 4. Typical vertical sequence and representative core photographs showing massive sand (*Lf*1) with floating mudstone clasts, interpreted to represent sandy debrite. B: bed base; T: bed top; Si: silt; Fs: fine sandstone; Cs: coarse sandstone. The well core location is given in Figures 1C and 8.

(Shanmugam *et al.*, 1993). The traction structures occurring in this lithofacies are interpreted to be the result of bottom-current reworking and represent alternating deposition events of traction and suspension (Shanmugam, 2003). Similarly, deep-water tidal deposits with double mud layers have been documented in modern and ancient sub-lacustrine sediments.

DEPOSITIONAL SYSTEM

Lithofacies association and distribution

After analyzing the vertical and lateral variations of the lithofacies from more than 300 wells, we reconstructed the spatial distribution of deep-lacustrine gravity flows

in the main profile (Fig. 8). The results show significant differences in lithofacies association, sandstone characteristics, and lateral distribution of lithofacies in the eastern and western depressions.

From proximal to distal deep-lacustrine areas, the thickness of the stratigraphic units and sediment grain size decrease (Fig. 8A). In the proximal area, the dominant composition is *Lf*3 deposits. For example, well W1 is composed mostly of coarse-grained massive sandstone with deformed bedding and locally interbedded mudstone. In deeper areas, the main lithofacies composition alternates between *Lf*1 and *Lf*2, whereas the typical *Lf*2 lithofacies with thinly bedded fine sandstone, siltstone and mudstone

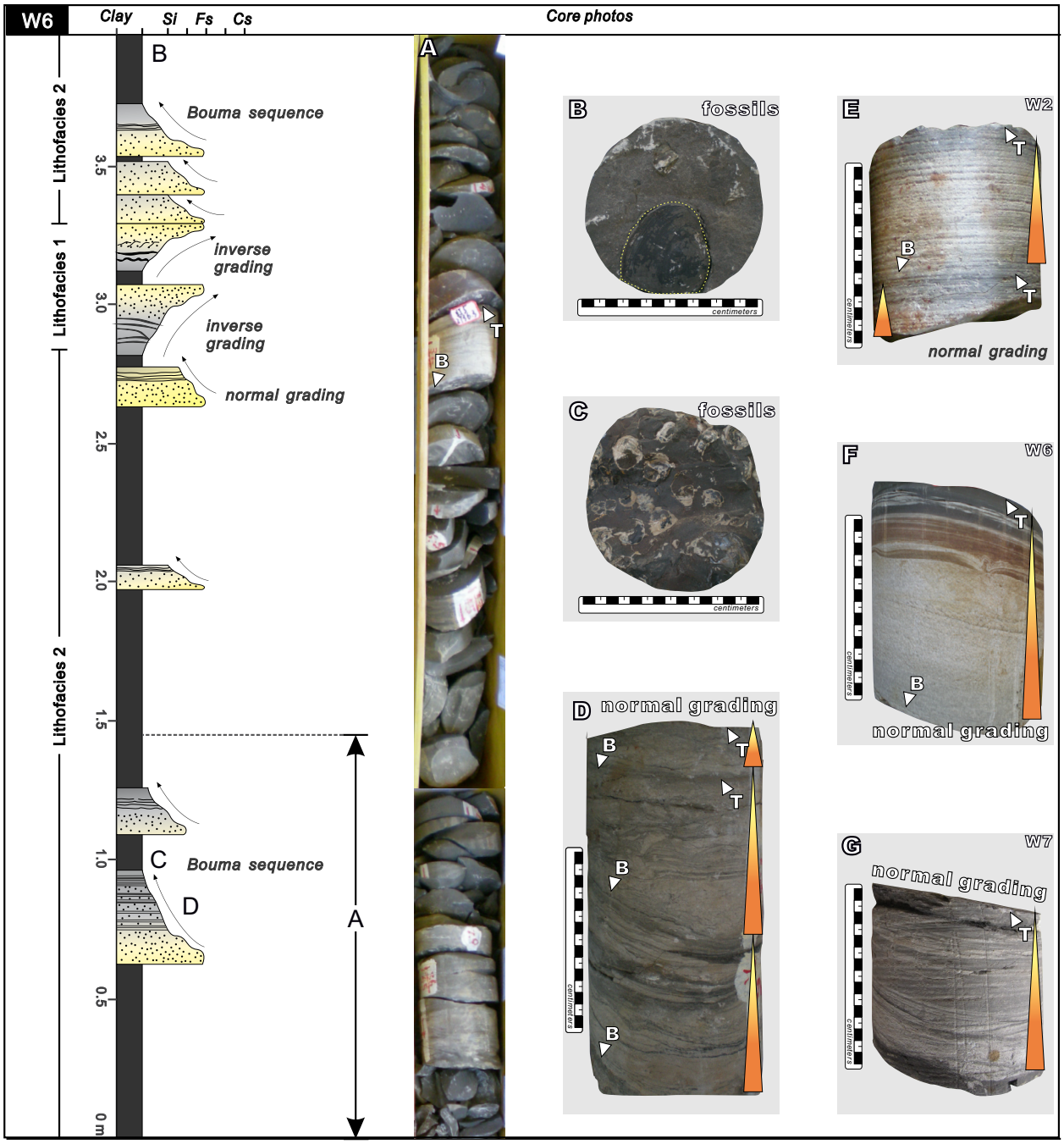

FIGURE 5. Typical vertical sequence and representative core photographs showing normal graded sandstone of *Lf2* interpreted to represent turbidite. *Lf2* and *Lf1* are vertically adjacent. B: bed base; T: bed top; Si: silt; Fs: fine sandstone; Cs: coarse sandstone. The core well locations are given in Figures 1C and 8.

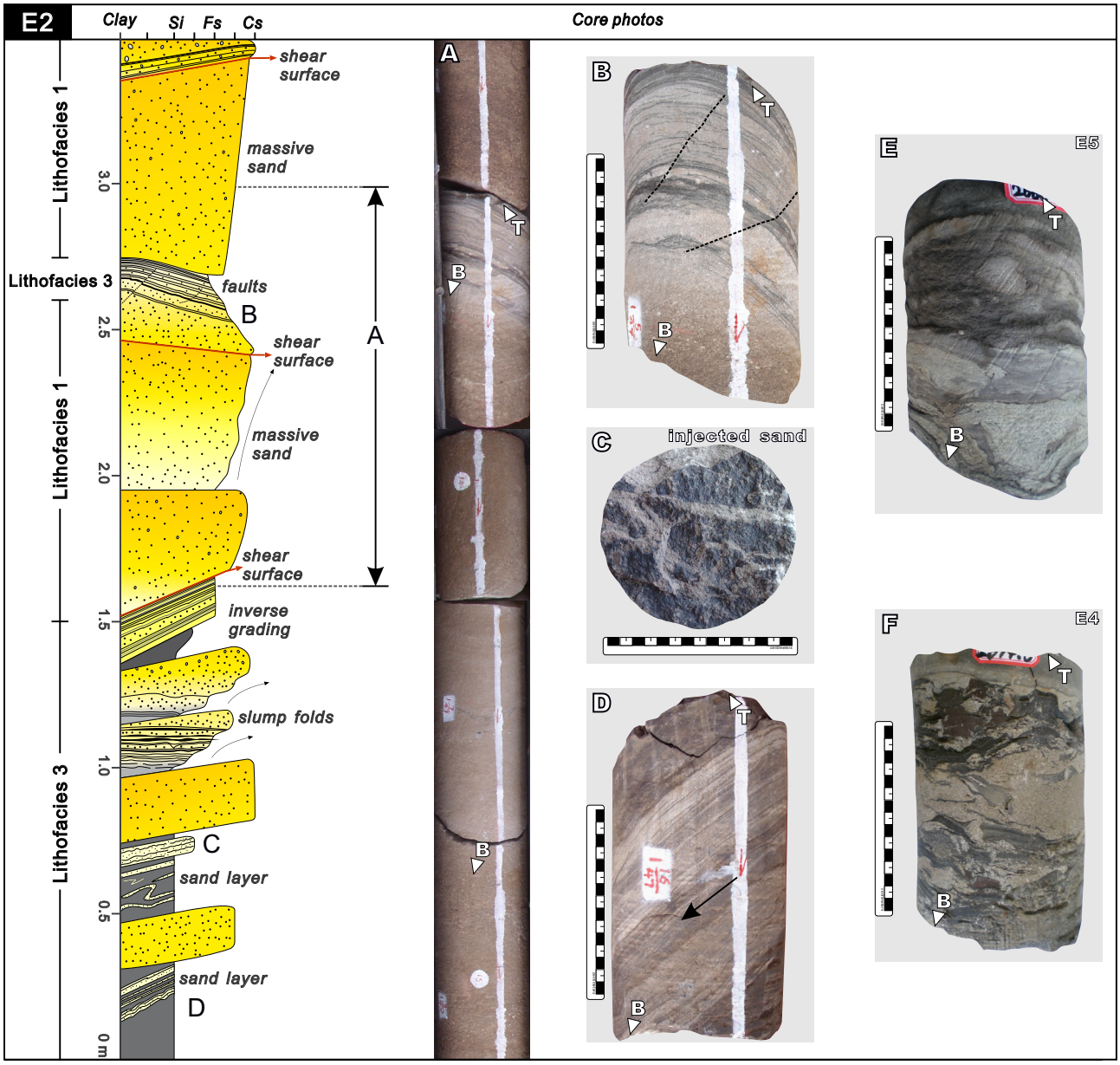

FIGURE 6. Typical vertical sequence and representative core photographs showing massive sandstone with a high degree of contortion and soft deformation, which is interpreted to be the sandy slump of *Lf*3. This lithofacies is vertically adjacent to *Lf*1. B: bed base; T: bed top; Si: silt; Fs: fine sandstone; Cs: coarse sandstone. The well core locations are given in Figures 1C and 8.

is developed in the deep-lacustrine area. Multiple stages of the Bouma sequence can also be identified in the core, which indicates gradual weakening of the hydrodynamic conditions and depositional environment dominated by turbidity currents (*e.g.* wells W7 and W8).

The sedimentary succession in the eastern depression (Fig. 8C) shows a grayish-white fine sandstone unit (*e.g.* well E1) at the slope break and a rapidly increases in thickness of the fine sandstone unit in the lower part of the slope break toward the basin, which is mainly composed of grayish-white coarse-medium sandstone with medium thickness. Core observations shows that typical *Lf*3 deposits are dominant (*e.g.* wells E3, E4 and E5). In the western region, however, the sedimentary succession is composed mainly of gray massive sandstone, although the sand layer shows a gradual decrease toward the deeper part of the basin. This lithofacies composition is typical of deep-lacustrine *Lf*1 deposits (*e.g.* wells E6, E7 and E8).

Sand dispersion system

Figure 8B shows that during the SQEls2EST + LST period, a facies belt with a sandstone content of up to 65%

developed from South to North of the southern slope belt, with its front end extended into the western depression. Small-scale, NE-trending sandstone belts with a maximum sand content of about 10% developed near well W7. In the eastern region, a small-scale belt with 40% maximum sand content developed from east to west. Near well E7, a small-scale North-South sand belt with a maximum sand content of 45% is present. The fault system has a main NE-SW trend and is developed mostly in the western depression. Sediments were supplied across the southern slope zone and dispersed along different paleocurrent directions. The main development was Northwestward; paleocurrents in the Northeastward and Southwestward directions developed at a smaller scale.

DEPOSITIONAL SYSTEM CHARACTERISTICS

Through comprehensive analysis of the lithofacies, changes in lithofacies assemblage, sand body dispersion system, and seismic data, we reconstructed the depositional system and its spatial distribution during the SQEls2EST

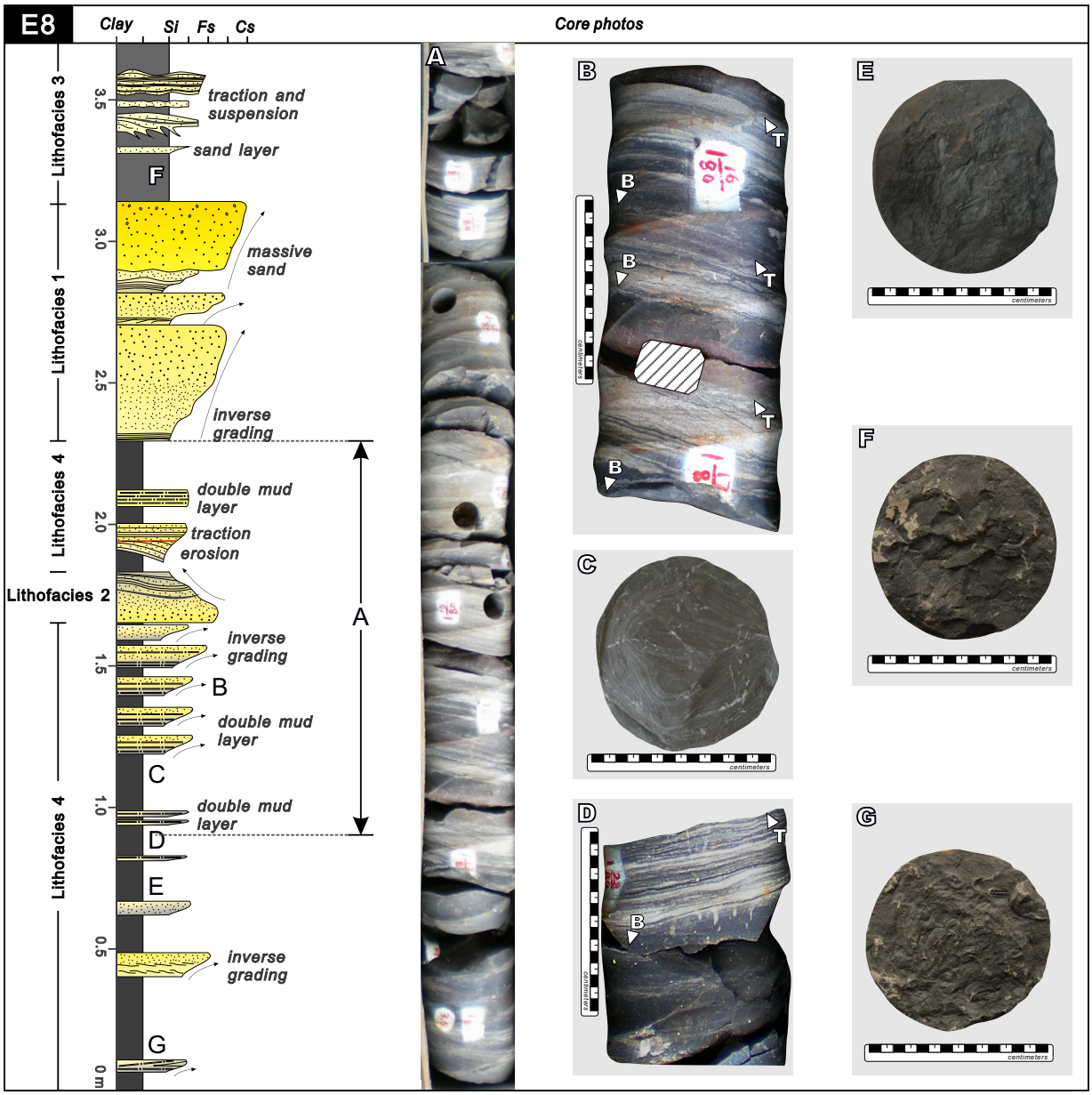

FIGURE 7. Typical vertical sequence and representative core photographs of ***Lf4*** showing mudstone intervals with the continuous presence of double mud layers interpreted to represent bottom-current. *Lf4* and *Lf2* are vertically adjacent. B: bed base; T: bed top; Si: silt; Fs: fine sandstone; Cs: coarse sandstone. The well core locations are given in Figures 1C and 8.

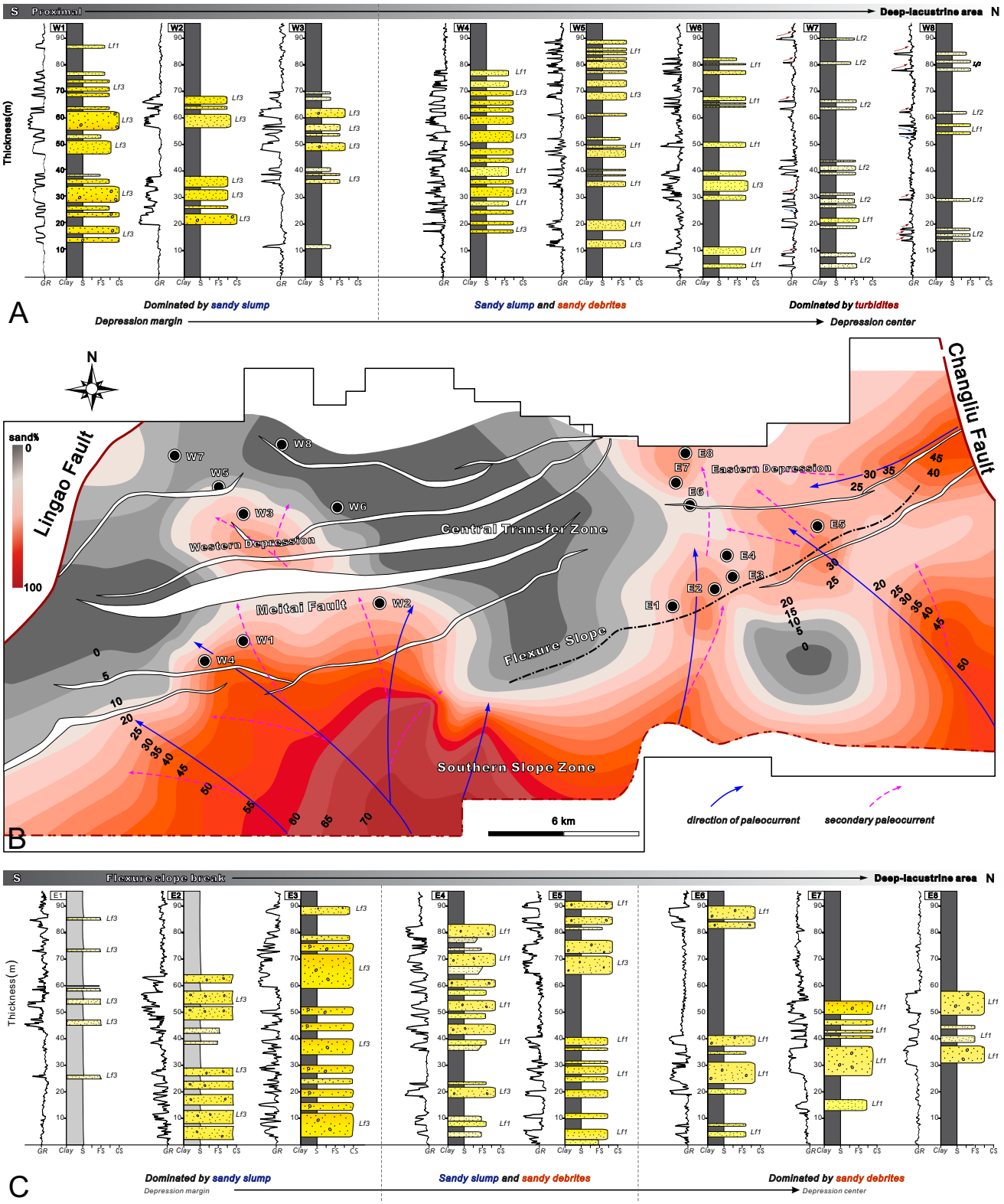

FIGURE 8. A) Lateral variation of lithofacies association in the western depression during the SQEIs2EST + LST period. B) Percentage of sandstone development during the SQEIs2EST + LST period. Contour lines indicate the paleocurrent direction and sandstone dispersion. C) Lateral relationships of lithofacies association in the eastern depression during the SQEIs2EST + LST period.

+ LST period. We calculated the basin subsidence through quantitative stratigraphic "back stripping method" to restore the paleogeomorphic base map (Li *et al.*, 2016), onto which the depositional system was superimposed.

The formation and evolution of the Fushan Sag occurred during the second episode of rift leading to a stage of regional lake expansion. The sag expanded to the maximum and the water body deepened rapidly in a quiet lacustrine sedimentary environment. Three depositional systems developed during this period: braided river delta, fan delta, and deep-lacustrine system dominated by gravity flow deposits (Fig. 9). The braided river delta largely dominated the depositional system in the western region and was distributed from the southern slope zone to the deep-lacustrine area. The braided river delta plain subfacies developed at a small scale. The braided river delta front subfacies are dominated by mouth bar deposits, and the distal bar is developed in the front of the mouth bar, indicating the delta's strong construction capacity. The eastern region of the sag is dominated by the braided river delta, which formed by the sediments from the Southeast uplift, whereas the smaller delta front deposits are developed in the central area. The fan delta deposits are developed mainly in the Yunlong uplift in the Northeast area, and the paleocurrent is relatively simple, presenting the characteristics of coarse clastic deposits under rapid accumulation. Overall, the provenance system in the eastern depression is weaker than that in the western depression.

Two different types of deep-lacustrine gravity flows produced different deposits in the eastern depression and the western depression. In the western depression, at the rolling anticline on the downthrow of the Meitai fault, sub-lacustrine fan deposits dominated by turbidity currents are developed with typical turbidite channels and fan-shaped external morphology. In the eastern depression, however, the isolated distal lobes were formed mainly by sandy debris flow deposition with no typical turbidite channels or the presence of a complete fan shape (Fig. 9).

BASIN STRUCTURAL STYLE AND DEPOSITIONAL MODEL

In a rifted lacustrine basin, the development of the depositional system depends on the distribution and migration history of sand sediments. The diffusion,

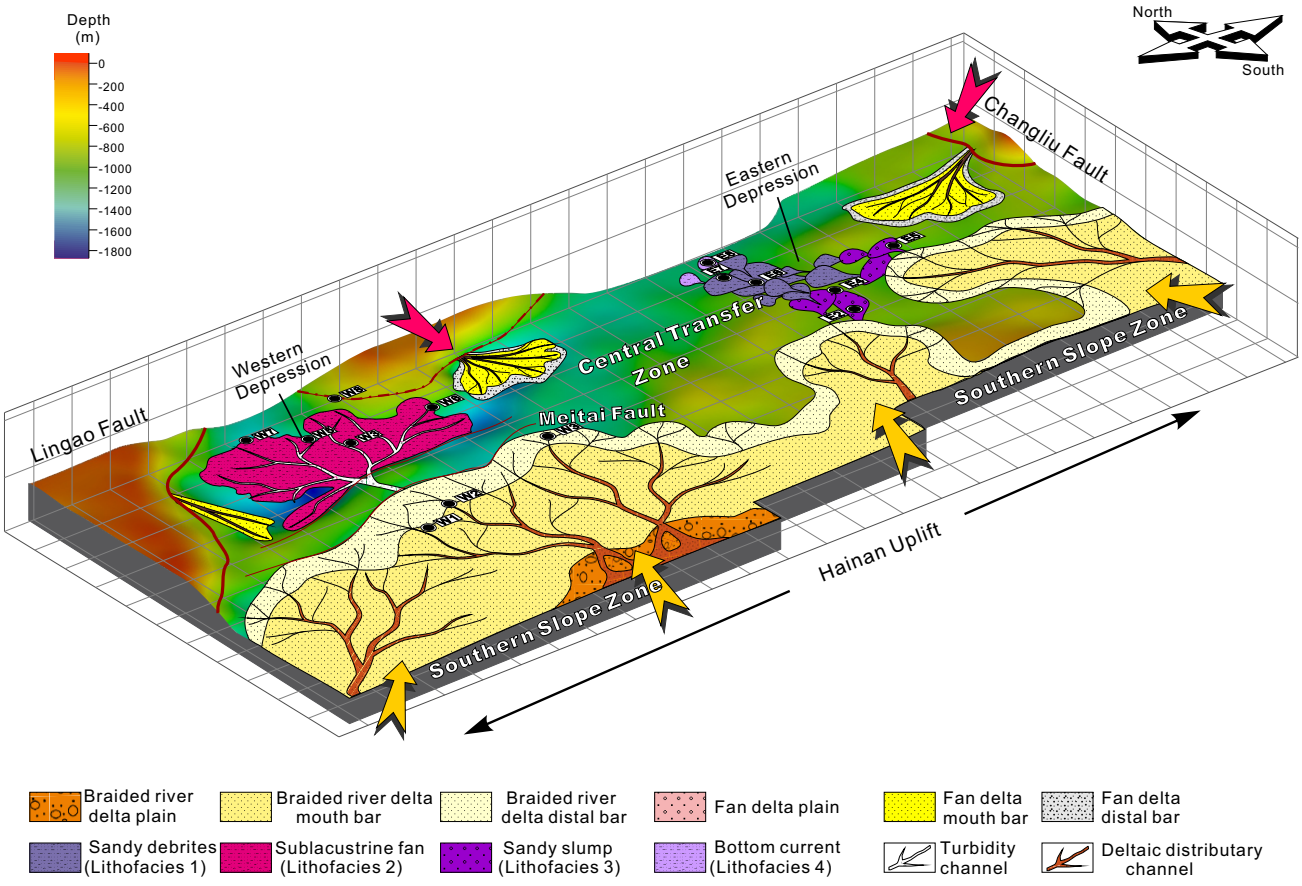

FIGURE 9. Distribution of depositional system composites on the contemporaneous palaeogeomorphology of SQEls2LST.

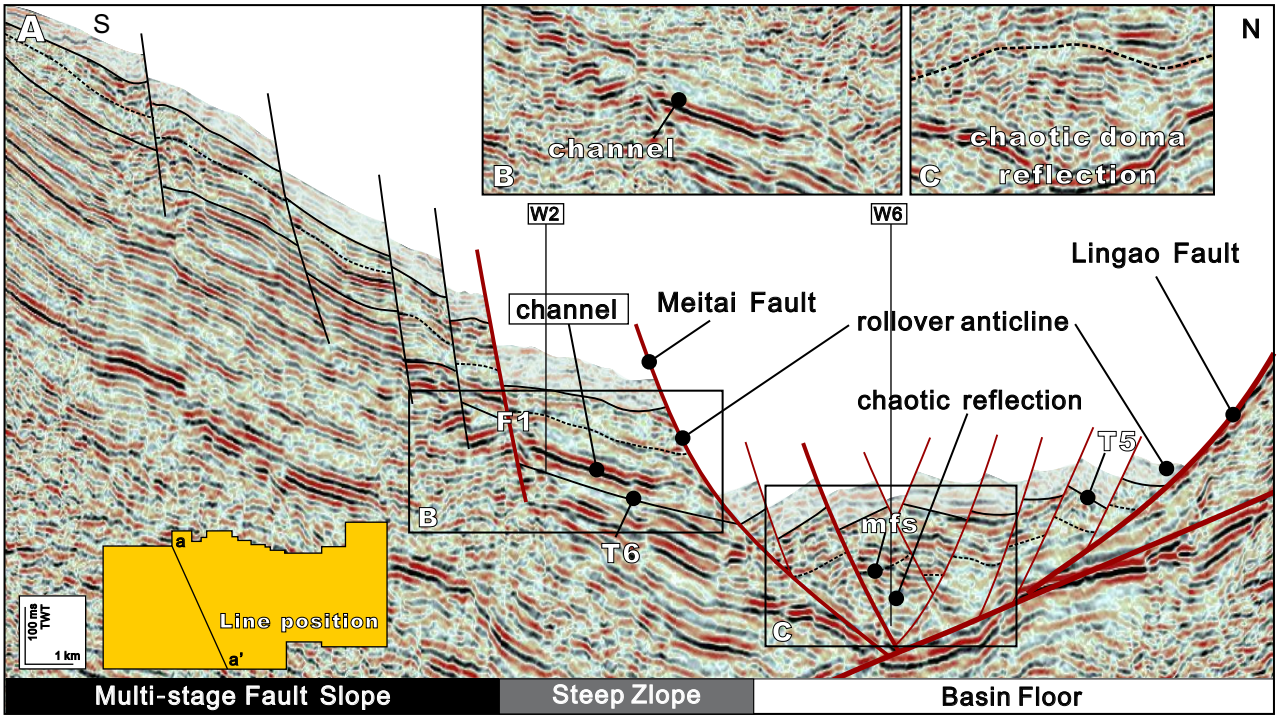

FIGURE 10. A) Seismic line showing the stratigraphic patterns of the western depression sequence divided by the Meitai fault into multistage fault slope and basin floor components. B) High-amplitude reflection showing channel seismic facies. C) Chaotic domal reflection assumed to be sub-lacustrine fan deposition.

transportation, and accumulation of these sediments are closely related to the structural style of the basin (Zhu *et al.*, 1993). Therefore, to understand the evolution of the deposition system, it is of great importance to analyze the sedimentary system-basin structural pattern under the sequence stratigraphic framework. Accordingly, we analyze the main structural styles of the eastern depression and the western depression and identified the corresponding depositional mode.

Sub-lacustrine fan setting

Western multistage fault terrace belt

During the SQEls2EST + LST period, the sequence structural style in the western depression was composed of two main parts. From the basin margin slope belt to the deep-lacustrine area, the multistage fault terrace belt and rolling anticline structure developed successively (Wang *et al.*, 2014) (Fig. 10). The main paleogeomorphic style of the southern slope zone was a multistage fault terrace belt, whereas mainly parallel faults developed in the western region. After entering the Paleogene, the rapid extension of the Fushan Sag and the activity of the Hainan uplift, under the influence of the basin-controlling Lingao fault, enabled the formation of the Meitai reverse secondary regulating fault. Among the multistage fault step zones, the fault distance at fault F1 began to increase until the fault distance of the Meitai fault reached its maximum. Syndepositional faults also had a profound effect on the sedimentation and stratigraphic formation. In this process, the secondary faults derived from the Lingao fault and the Meitai fault were adjusted, thus forming the double traction rolling anticline structure in the western deep-lacustrine area, which received its material supply from multiple directions.

Depositional model of sub-lacustrine fan

In the western depression, the multistage fault terrace was the main location of the events triggering gravity flow. The concave bottom formed by the rolling anticline was the main unloading point for deep-lacustrine gravity flow deposits, whereas the long and gentle slope belt between the multistage fault terrace and the rolling anticline was the transportation area for these deposits. Figure 11 illustrates the proposed depositional model for the western depression. During the differential transport process of the delta front deposit, the water body at the top gradually mixed with the lower part and formed a turbidity current after turbulence transformation, which enabled the mixed fluid to continue the transport to the deep-lacustrine area. In front of the deltaic deposition, the model included three stages. First, when the turbidity reached the first-order fault at the down-dropped block of the Meitai fault, its energy decreased owing to the fault resistance. Most of the turbidity at the

bottom crossed the slope break zone under the influence of turbulent transportation to form large-scale contiguous sedimentary bodies in the deep-lacustrine area. This flow was dominated by turbidites with normal grading, which is analogous to the channelized turbidite model of Lake Baikal (Nelson, 1999) (Fig. 11A). Second, as the hydrodynamic condition weakened, the movement of the channelized turbidite fan decreased (Fig. 11B). Third, the hydrodynamic energy weakened enough to form low-density turbidity currents that passed the extension antithetic fault terraces, which are interpreted as non-channelized turbidite deposits (Fig. 11C). When turbidity currents are inherently low in sediment concentration, true high-density turbidity currents cannot exist. Thus, we distinguished only normal and low-density turbidity currents in the basin floor area.

Our model is analogous to the conventional turbidite fan model (Nilsen, 1980; Walker, 1978) which includes turbulent and low-density turbidity currents. According to the sandstone content of 33%-70% in the sub-lacustrine depositional system in the western depression, our sub-lacustrine fan is closer in similarity to the sand-rich sub-marine fan model (Reading and Richards, 1994) based on a small-scale fan composed of the deposits transported from the sand-rich continental shelf through incised valleys or faults with distribution controlled mainly by tectonic patterns. Considering the tiny displacement of the faults in the rollover anticline system and natural safety barriers (Chen, 1999; Poblet, 2007) on both sides (Meitai fault and Lingao fault), we determined that the depositional environment for sub-lacustrine turbidite fan in the western depression was flat and quiet.

During the SQEls2EST + LST period, the sub-lacustrine fan deposits were distributed mainly in the deep-lacustrine part of the downthrow of the Meitai fault in the western depression. In the plane distribution, with the Meitai fault serving as the dividing line, the sub-lacustrine fan was distributed in front of the braided river delta front deposits to occupy the lacustrine area of the western depression. Influenced by faults in the W-E direction, the sub-lacustrine fan tended to migrate from the West to the East. The fan body is overall symmetrical, which indicates homogeneity of the sedimentary topography and the characteristics of a single-channel supply source (Fig. 11).

Sandy debrites setting

Eastern flexure slope break

The fault activity is weaker in the eastern depression, which had a smaller influence on the transformation of the original slope zone and the distribution of sedimentary sand. In addition, the flexure slope break zone is widely developed in this area (Fig. 12) (Ma *et al.*, 2012). The flexure slope break zone was formed

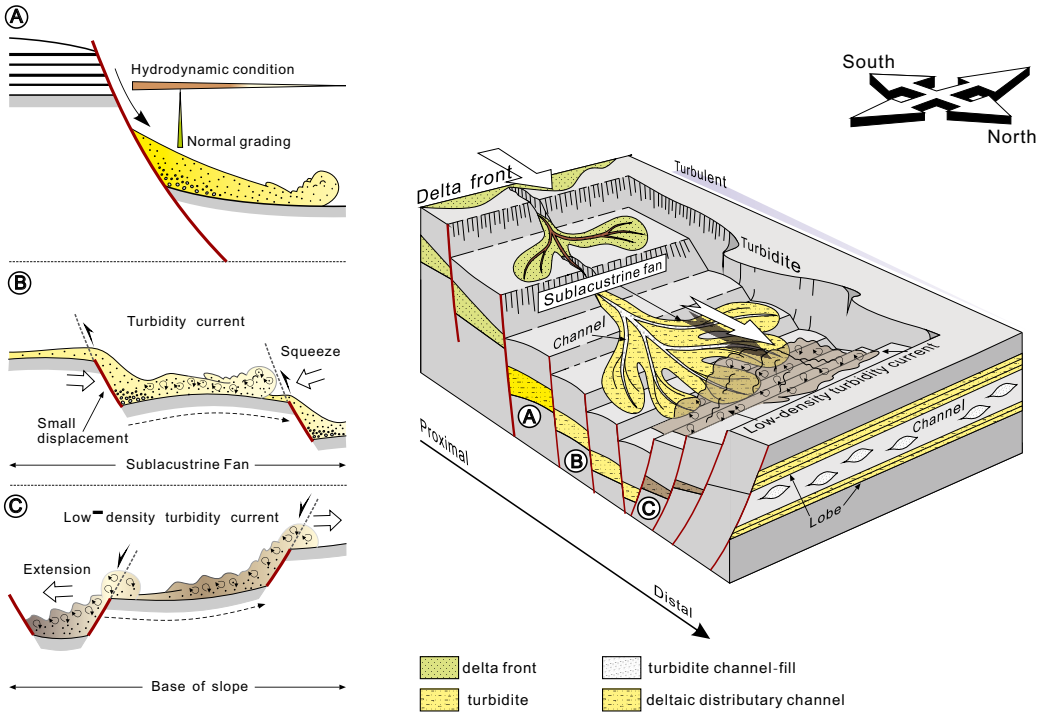

FIGURE 11. A Formation mechanism model of the western sub-lacustrine fan setting including turbidite channels and lobes deposited dominantly by turbulent flows. A, B and C represent three turbidite-phase lithofacies, respectively, which indicate weakening of the hydrodynamic conditions toward the basin floor area.

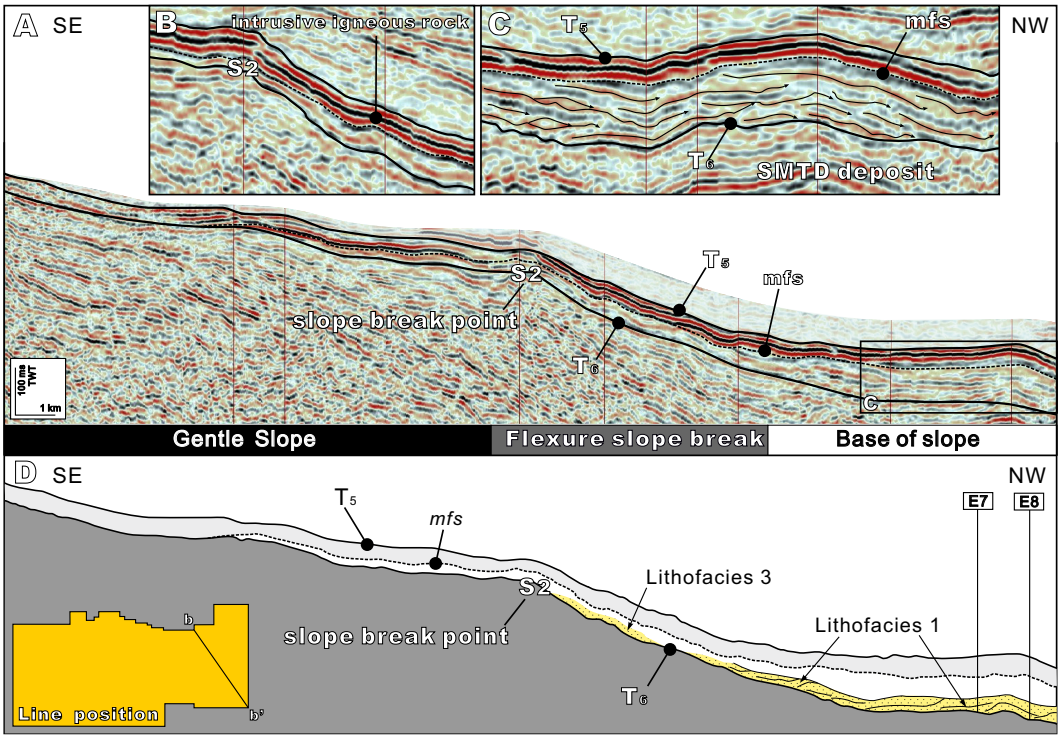

FIGURE 12. A) Seismic line showing the stratigraphic pattern of the eastern depression sequence, which is divided into three main components: gentle slope, flexure slope break, and slope base. The maximum flooding surface (mfs) is revealed in the seismic section by combining the using lithologic logs. B) Chaotic low-amplitude reflection representing intrusive igneous rock. C) Chaotic low-amplitude reflection with continuous high-amplitude reflection interpreted as sandy debrites deposition. D) Schematic cross-profile showing mapped horizons, borehole locations, and general sediments distribution of the SQEls2EST + LST period. SMTD: sand mass transport deposition.

generally on the early hidden faults with typical flexure slope break points, which can be considered as a transitional style between the slope type and the fault block paleogeomorphology. The flexure slope break zone developed early in the SQEls2 period and is distributed mainly in the southern slope zone of the eastern depression. The specific distribution range extends from the southern to Southeast slope zones. The seismic profiles show that the stratum thickness is lowest at the slope break point and increases after crossing the slope break point. The slope break point divides the slope into three components: a gentle slope zone near the sub-basin margin, a flexure slope break belt, and the slope base. The slope break in the eastern region is more gentle than that in the western region, and the slope area below the slope break is longer, which provides sufficient slope area and length for the formation of a sandy debris flow (Fig. 12).

Depositional model of sandy debrites

Figure 13 illustrates the proposed depositional model of sandy debrite in the eastern depression. In front of the deltaic deposition, the model is composed of three parts. First, in the area close to the flexure slope break point, as the slope germinates and hinders the further transportation of the braided river delta in the upstream side of slope break, the proximal area in the downstream side of the slope break is dominated by the sandy slump of *Lf*3 (Fig. 13A). The term "slump" in the case refers to both the process and the deposit, which is interpreted to be a coherent mass of sediment that moved on a concave-up glide plane and underwent rotational movement, causing internal deformation (Shanmugam, 2009, 2013). Second, sandy debrites dominate the area between the gentle slope and the base of slope zone, which is similar to the non-channelized debrite model of Shanmugam (2000) and Zou (2012). The recognition of sandy debrites in this study conflicts with the results of previous research of channelized turbidite fan deposition. In addition to the lack of turbidite channels, the topography, coarse granularity, high sediment concentration, inverse grading, floating mudstone clasts, and sharp and irregular upper contacts exclude the presence of turbidity currents (Fig. 13B). Third, as a laminar flow transfers into turbulent flow, from the base of the slope to the basin floor area, turbidity currents are generated with parts being reworked by bottom-current (Fig. 13C). Therefore, isolated or lenticles deposits occur in the eastern seismic profiles.

DISCUSSION

Formation conditions of deep-lacustrine gravity flow

During the SQEls2EST + LST period, the intensified rifting activity led to the rapid expansion of the sag followed by a rapid increase of subsidence thus forming a deep-lacustrine environment. During the development of the Liushagang Formation, the main source of the sediments was the southern Hainan uplift. The topography of the study area is a wide and gentle landform inclined towards the South (Fig. 2C), which created favorable topographic conditions for the development of deep-water gravity flows. During the early stage of the SQEls2 period, the drainage system developed progressively, and the deltaic system prograded onto the lake basin, providing with the material for the formation of sandy debris flows. Finally, during the Paleogene period, volcanic activity occurred in the Fushan Sag region. Violent volcanic eruptions triggered frequent earthquakes, and multistage flooding that occurred during the maximum lake expansion period provided a trigger mechanism for the formation of gravity flows. In summary, the high sediment supply, slope structure, and volcanic and seismic activities provided favorable conditions for the formation of deep-lacustrine gravity flow deposits in the Fushan Sag.

Difference analysis of deep-lacustrine gravity flow

Deposition system. During the SQEls2EST + LST period, the braided river delta front prograded and reached the Meitai fault near the basin center, leading to the formation of a more extensive and farther advanced far-sand dam deposit with finer-grained sediments. In contrast, the delta front in the eastern region did not advance to the deep-lacustrine area; instead, the sediments accumulated above the flexure slope break zone. The sandy debrites were formed by the reworking of sand-rich braided channel-estuarine bar sediments. The sediment is coarser and the sandstone layers are thicker in the eastern region than those of the distant sand bar in the western region.

Basin structural style

During the SQEls2EST + LST period, tectonic activity along the Central Transfer Zone led to the basin partitioning, resulting in differential subsidence and different structural styles in the eastern depression and the western depression. The slope break served as the hinge of the sediment energy change. In the western depression, under the control of the multistage fault terrace, the sediments were graded several times. Thus, only fine sediments reached the deep-lacustrine area to form a turbidite fan. In the eastern depression, however, the slope is relatively gentle. Most

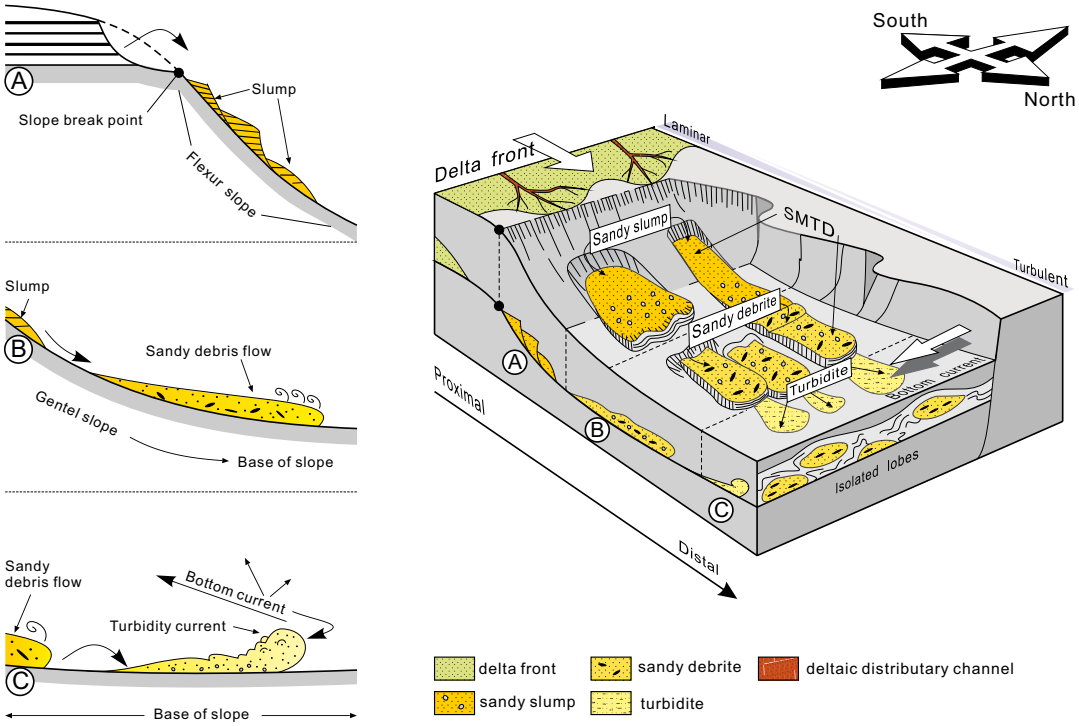

FIGURE 13. Sedimentary model for the formation of sandy debrites in the eastern region. Deposits range from sandy slumps to sandy debrites originated from dominantly laminar flows, which in turn generates turbidites on the basin floor. A, B and C represent the three types of gravity flow lithofacies, respectively. SMTD: sand mass transport deposition.

of the sediment in this area crossed the slope break point to reach the deep-lacustrine area. Therefore, the eastern depression is composed mainly of isolated coarser sand units.

CONCLUSIONS

Through observation of 16 cores obtained in the deep-lacustrine area of the Fushan Sag, we determined that four types of deep-lacustrine gravity flow lithofacies formed during the SQEls2EST + LST period: sandy debrites, turbidites, sandy slumps, and bottom-current deposits. The sediment grain size, genetic mechanism, and rheological properties differ among the lithofacies.

From the near source area to the deep-lacustrine area in the western depression, the sedimentary succession exhibits gradual changes from thick to thin layers and coarse to fine sediment, which reflects the sedimentary environment of a quiet water body, low-energy hydrodynamic conditions, and dominated by turbidity currents. In the eastern region, the thickness of the sand body increases rapidly in the lower part of the slope toward the basin and the lithology is mainly gray to white medium-coarse sandstone of medium thickness, which is typical of deep-water sandy debris flow deposits.

During the SQEls2EST + LST depositional period, two different structural styles developed in the eastern depression and the western depression of the Fushan Sag. In the western region a multistage fault terrace belt and a rolling anticline structure developed successively from the slope belt of basin margin to the deep-lacustrine area. In the eastern depression, however, the fault activity had little influence on the transformation of the original slope zone and the distribution of sediments, and the structural style of a flexure slope break zone is dominant.

Two different types of deep-lacustrine gravity flow developed in the two depressions during the SQEls2EST + LST period. In the western region, sub-lacustrine fan deposits dominated by turbidity currents developed, with typical turbidite channel deposits and fan shaped lobes. In the eastern region, however, the isolated distal lobes were formed mainly by sandy debris flow deposition and do not exhibit typical turbidite channels or fan-shaped lobes.

Generally speaking, the differences in deep-water gravity flow deposition between the eastern depression and the western depression were caused by the distance to the sediment source, the water depth, the steepness of the slope break and the length of slope area below the slope break, and the basin floor topography at the deposition site.

ACKNOWLEDGMENTS

The authors thank the Scientific Research Fund of the Institute of Seismology, CEA, and the National Institute of Natural Hazards, Ministry of Emergency Management of China (Grant No.IS201626261), for funding this study and allowing its publication. In addition, the China Southern Petroleum Exploration & Development Corporation is thanked for allowing publication of the well log and seismic data. The authors also thank Professor Hua Wang and Professor R.W.C. Arnott for providing instruction and discussion, as well as Laura Rincón, Daniel Ariztegui, and Ovie Emmanuel Eruteya for providing constructive and comprehensive reviews that helped to improve this manuscript. We thank International Science Editing for editing this manuscript.

REFERENCES

Bouma, A.H., 1962. Sedimentology of some flysch deposits: a graphic approach to facies interpretation. Amsterdam, Elsevier, 168pp.

Chen, S.P., Wang, Z.B., Liu, E.J., 1999. Study on rollover anticline in Zhanche area. Journal of the University of Petroleum, 23(3), 6-12.

Elverhoi, A., Issler, D., Blasio, F., Ilstad, T., Harbitz, C.B., Gauer, P., 2005. Emerging insights into the dynamics of submarine debris flows. Natural Hazards and Earth System Sciences, 5(3), 633-648.

Forel, M., 1887. 'Ravins sous-lacustres des fleuves glaciaires'. Comptes rendus de l'Academie des Sciences, 101, 725-728.

He, Y.B., Gao, Z.Z., 2006. Sedimentary facies of the Liushagang Formation of Paleogene in Fushan depression of Hainan Island. Journal of Palaeogeography-China, 8(3), 365-376.

Johnson, D., 1938. The origin of submarine canyons. Journal of Geomorphology, 1, 111-340.

Kang, X.D., Zhao, W.C., Pan, Z.G., 1994. Study on architecture of sequence stratigraphic framework of Beibuwan Basin. Journal of Earth Science, 19(4), 493-502.

Li, Y., Liu, J., Ma, Q.L., 2010. Sedimentary characteristics of gravity flows in Paleogene Liu 1 formation of the Fushan Depression. Special Oil and Gas Reservoirs, 17(5), 30-33.

Li, Y., Wang, H., Liu, E.T., Liao, Y.T., Lin, Z.L., Ma, Q.L., 2014. Distribution regularities and control factors for reservoir formation within sequence stratigraphic framework in Fushan Sag, Beibuwan Basin. Journal of Central South University (Science and Technology), 45(5), 1542-1554.

Li, Y., Zhao, Y.N., Lin, Z.L., Ma, Q.L., 2016. Tectonic characteristics and structural styles of a continental rifted basin: revelation from deep seismic reflection profiles. Geodesy and Geodynamics, 5, 329-339.

Li, X.B, Liu, H.Q., Pan, S.X., Wang, J., 2019. The past, present and future of research on deep-water sedimentary gravity flow in lake basins of China. Acta Sedimentologica Sinica, 37(5), 904-921.

Lin, Z.L., Wang, H., Li, H.J., Ma, Q.L., Li, Y., Zhao, S.E., 2015. Genetic mechanism of double-layer structure in Paleogene of

Fushan depression, Beibuwan Basin. Journal of Earth Science, 40(1), 169-178.

Liu, J.P., Xian, B.Z., Wang, J.H., Ji, Y.L., Lu, Z.Y., Liu, S.J., 2017. Sedimentary architecture of a sub-lacustrine debris fan: Eocene Dongying Depression, Bohai Bay Basin, East China. Sedimentary Geology, 362, 66-82.

Liu, L.J., Gao, Z.Z., 2000. Research on depositional system and reservoir prediction of Paleogene stratum in the Fushan Depression, Hainan Province. Earth Science Frontiers, 7(4), 390.

Liu, L.J., Tong, Y.M., Ji, Y.L., 2003. Sedimentary characteristics and developing background of the sub-lacustrine fan in the Liushagang formation of the Fushan Depression, the Beibuwan basin. Petroleum geology and experiment, 25(2), 110-115.

Luo, J.X., He, Y.B., Gao, Z.Z., 2007. Gravity flows deposits of Paleogene Liushagang Formation in Fushan depression, Hainan Province. Offshore Oil, 27(3), 9-14.

Ma, Q.L, Zhao, S.E., Liao, Y.T., Lin, Z.L., 2012. Sequence architectures of Paleogene Liushagang Formation and its significance in Fushan Sag of the Beibuwan Basin. Journal of Earth Science, 37(4), 667-678.

Nelson, C.H., Karabanov, E.B., Colman, S.M., Escutia, C., 1999. Tectonic and sediment supply control of deep rifted lake turbidite systems: Lake Baikal, Russia. Geology, 27(2), 163-166.

Nilsen, T.H., 1980. Modern and ancient submarine fans: discussion of papers by R.G. Walker and W.R. Normark. American Association of Petroleum Geologists Bulletin, 64(7), 1094-1101.

Pan, S.X., Liu, H.Q., Zavala, C., Liu, C.Y., Liang, S.J., 2017. Sub-lacustrine hyperpycnal channel-fan system in a large depression basin: A case study of Nen 1 Member, Cretaceous Nenjiang Formation in the Songliao Basin, NE China. Petroleum Exploration and Development, 44(6), 860-870.

Poblet, J., Bulnes, M., 2007. Predicting strain using forward modelling of restored cross-sections: Application to rollover anticlines over listric normal faults. Journal of Structural Geology, 29(12), 1960-1970.

Reading, H.G., Richards, M., 1994. Turbidite systems in deep-water basin margings classified by grain size and feeder system. American Association of Petroleum Geologists (AAPG) Bulletin, 78(5), 792-822.

Shanmugam, G., Spalding, T.D., Rofheart, D.H., 1993. Process sedimentology and reservoir quality of deep-marine bottom-current reworked sands (sandy contourites): an example from the Gulf of Mexico. American Association of Petroleum Geologists (AAPG) Bulletin, 77(1), 1241-1259.

Shanmugam, G., 2003. Deep-marine tidal bottom currents and their reworked sands in modern and ancient submarine canyons. Marine and Petroleum Geology, 20, 471-491.

Shanmugam G., 1996. High-density turbidity currents: are they sandy debris flows? Journal of Sedimentary Research, 66(1), 2-10.

Shanmugam, G., 1997. The Bouma Sequence and the turbidite mind set. Earth-Science Reviews, 42(4), 201-229.

Shanmugam, G., 2000. 50 years of the turbidite paradigm (1950s-1990s): deep-water processes and facies models - a critical perspective. Marine and Petroleum Geology, 17(2), 285-342.

Shanmugam, G., Shrivastava, S.K., Das, B., 2009. Sandy debrites and tidalites of Pliocene reservoir sands in upper-slope canyon environments, Offshore Krishna Godavari Basin (India). Journal of Sedimentary Research, 79, 736-756.

Shanmugam, G., 2013. New perspectives on deep-water sandstones. Petroleum Exploration and Development, 40(3), 316-324.

Sheldon, P.G., 1928. Some sedimentation conditions in Middle Portage rocks. American Journal of Science, 15(87), 243-252.

Shi, Y.M., Liu, J., Zhang, M.Z., Chen, D.X., Ma, Q.L., 2007. Experience and understand in oil and gas exploration in Fushan depression, Hainan Province, South China. Journal of Seismology, 27(3), 57-68.

Vail, P.R., 1987. Seismic stratigraphic interpretation procedure. In: Bally, A.W. (ed.). Atlas of Seismic Stratigraphy. American Association of Petroleum Geologists (AAPG) Bulletin, 27, 1-10.

Walker, R.G., 1978. Deep-water sandstone facies and ancient submarine fans: models for exploration for stratigraphic traps. The American Association of Petroleum Geologists Bulletin, 62(6), 932-966.

Wang, G.H., Huang, C.Y., Liu, E.T., Li, Y., Pan, S.Q., 2014. Characteristics of slope-breaks and its control on sedimentation and hydrocarbon accumulation of Liushagang Formation in gentle slope of south Fushan sag. Journal of Central South University (Science and Technology), 45(5), 1531-1541.

Xian, B.Z., Wan, J.F., Jiang, Z.X., Zhang, J.G., Li, Z.P., She, Y.Q., 2012. Sedimentary characteristics and model of gravity flow deposition in the depressed belt of rift lacustrine basin: a case study from Dongying Formation in Nanpu Depression. Earth Science Frontiers, 19(1), 121-135.

Xian, B.Z., Wang, L., Liu, J.P., Lu, Z.Y., Niu, S.W., Zhu, Y.F., Hong, F.H., 2016. Sedimentary characteristics and model of delta-fed turbidites in Eocene eastern Dongying Depression. Journal of China University of Petroleum, 40(5), 10-21.

Yang, R.C., He, Z.L., Qiu, G.Q., Jin, Z.J., Sun, D.S., Jin, X.H., 2014. Late Triassic gravity flow depositional systems in the southern Ordos Basin. Petroleum Exploration and Development, 41(6), 661-670.

Yang, T., Cao, Y.C., Wang, Y.Z., Zhang, S.M., 2015. Types, sedimentary characteristics and genetic mechanisms of deep-water gravity flows: a case study of the middle submember in Member 3 of Shahejie Formation in Jiyang Depression. Acta Petrolei Sinica, 36(9), 1048-1059.

Zhu, Z.Q., Lin, C.Y., Zhang, X.G., Li, Z.P., Xie, J.J., Wei, S.D., Chen, P., 2017. Shallow water delta deposits in a rifting lacustrine basin during early stage: a case study of the first member of Dainan Formation at Yong'an area, Gaoyou Sag. Journal of Jilin University (Earth Science Edition), 47(3), 659-673.

Zou, C.N., Wang, L., Li, Y., Tao, S., Hou, L., 2012. Deep-lacustrine transformation of sandy debrites into turbidites, Upper Triassic, Central China. Sedimentary Geology, 265, 143-155.

Manuscript received December 2020;
revision accepted December 2021;
published Online March 2022.